AD-A191 090 PRELIMINARY MEASUREMENTS OF HEAT FLUX IN A SUBSONIC GUN SIMULATOR(U) IMPERIAL COLL OF SCIENCE AND TECHNOLOGY LONDON (ENGLAND) DEPT.. A F BICEN ET AL. DEC 87 1/1

UNCLASSIFIED DAJA45-87-C-0045 F/G 20/12 NL

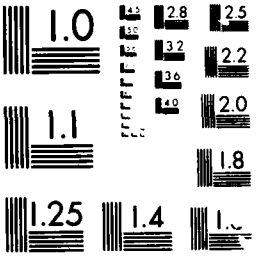

IMPERIAL COLLEGE OF SCIENCE & TECHNOLOGY
Mechanical Engineering Department, Fluids Section
Exhibition Road, London SW7 2BX, England

Preliminary Measurements of Heat Flux in a Subsonic Gun Simulator

First Interim Report

by

A F Bicen, M Schmidt, and J H Whitelaw

December 1987

United States Army
European Research Office of the US Army
London, England

Contract Number DAJA 45-87-C-0045

Approved for Public Release; distribution unlimited

FS/87/39

ABSTRACT

Preliminary measurements of heat flux have been obtained in a subsonic gun simulator with thin-film resistance thermometry for an inert, single-phase flow expanding behind a projectile from an initial pressure of 8 bars and resulting in an exit projectile velocity of 40 m/s. The results show that heat transfer measurements at locations swept by the projectile are possible using thin-film sensors set into the wall by 0.1 mm and that the heat flux at various axial locations decreases with time and increases with distance from the breech. The measured convection coefficients at locations swept by the projectile differ up to 50% from those evaluated with quasi-steady flow assumption from a correlation for turbulent boundary layer with zero pressure gradient starting at the breech, due to the neglect of pressure gradient as well as to the effect of projectile wake on the boundary layer development. In the initial chamber, the projectile wake effect is insignificant and as the pressure gradient reduces during the later stages of the shot, the measured values approach the correlation results and achieve values within 10%.

1. INTRODUCTION

The flow field behind the projectile of the gun simulator is described in references 1 to 3. In reference 1, LDA measurements are reported for a single-phase flow and indicated that the velocity boundary layers were turbulent and occupied up to 20% of the barrel radius. The corresponding measurements in the presence of 500 μm particles of various initial concentrations are reported in references 2 and 3. The present work is concerned with the heat transfer process of the single-phase flow in the gun-simulator of reference 1. The main objective of the work is to obtain information on the nature of the heat transfer process and thermal boundary layers as well as to provide guidance for more detailed measurements of heat transfer with improved instrumentation in the present rig and in a high speed rig with single- and two-phase flows.

2. EXPERIMENTAL SYSTEM

2.1 Flow Configuration

The gun simulator shown in Figure 1 is similar to that of references 1 to 3 and its geometric details can be found there. A brief description of the flow arrangement is given below.

At the beginning of a shot, the projectile of the gun simulator is secured by a lock mechanism in position inside a barrel of 76.5 mm diameter and its initial chamber of the same diameter is pressurised by compressed nitrogen to 8 bars (gauge). After the gas becomes quiescent, the projectile

is released and travels a distance of about 1 m in about 33 ms, reaching an exit velocity of 40 m/s. At the end of its travel, the projectile is decelerated by compression of air inside the lower part of the barrel and is subsequently returned to its start position at the top for a new shot.

2.2 Heat Transfer Instrumentation

Heat transfer measurements at various axial locations along the barrel have been obtained by using a fast-response thin-film resistance thermometer (Dantec 55R47). The sensor has a thin Nickel film of about 100^{o}A thick, 1 mm long and 0.1 mm wide on a 50 μm thick insulator substrate of Kapton. The electrical resistance of the film changes with temperature and provides a measure of the surface temperature of the substrate. The resistance of the film was measured with a constant-current circuit, the output voltage of which is proportional to the sensor resistance. The output of the circuit was amplified (x2000), digitised and interfaced to a microcomputer which recorded the time-resolved sensor temperature data during each shot. A pulse obtained from the photodiode/laser arrangement shown in Figure 1 was used to initiate the microcomputer to record the data at the beginning of each shot. The initial chamber pressure was measured by a pressure transducer and a charge amplifier and monitored for each shot as a check on the repeatability of the experiments.

Time-resolved heat flux during a shot can be evaluated using the measured temperature data according to the procedure described in reference 4. Assuming one-dimensional heat conduction and ignoring the effect of finite film and substrate thicknesses on heat conduction process, the heat flux, q, can be shown to be related to the surface temperature of the substrate as:

$$\dot{q}(t) = \sqrt{\frac{\rho c k}{\pi}} \left\{ \frac{T(t)}{\sqrt{t}} + \frac{1}{2} \int_0^t \frac{T(t)-T(\tau)}{(t-\tau)^{3/2}} \, d\tau \right\} \qquad (1)$$

where ρ, c and k are the density, specific heat and thermal conductivity of the substrate material, T the change in the substrate temperature, t the time and τ is the time variable of the integration.

In this form there is, however, a singularity in the integral term at $t = \tau$ which will give rise to errors in the deduced values of $\dot{q}$. These errors can be reduced by approximating the above equation numerically by:

$$\dot{q}_n(t) = \sqrt{\frac{\rho c k}{\pi}} \left\{ \frac{T(t_n)}{\sqrt{t_n}} + \sum_{i=1}^{n-1} \left(\frac{T(t_n)-T(t_i)}{(t_n-t_i)^{\frac{1}{2}}} - \frac{T(t_n)-T(t_{i-1})}{(t_n-t_{i-1})^{\frac{1}{2}}} + 2 \frac{T(t_i)-T(t_{i-1})}{(t_n-t_i)^{\frac{1}{2}}+(t_n-t_{i-1})^{\frac{1}{2}}} \right) + \frac{T(t_n)-T(t_{n-1})}{\sqrt{\Delta t}} \right\} \qquad (2)$$

The sensor has a dynamic response of less than 1 μs for 63% of a step input. The output of the amplifier is, however, limited to around 8 KHz at -3 dB and the microcomputer can sample the signal at a rate of about 10 KHz. The dynamic response of the system as a whole is fast relative to the time-resolved temperature variation during a shot lasting for about 33 ms. The overall noise level of the system was of the order of 25 mV peak-to-peak and corresponded to a temperature uncertainty of about ± 0.3°C, which represents about ± 5% of the maximum temperature change achieved during the shot.

3. RESULTS AND DISCUSSION

In this section measurements obtained at various axial locations corresponding to distances from the breech of x = 2.88d, 7.27d, 10.21d, 13.15d and 16.09d are presented. The first position (x = 2.88d) corresponds to a location inside the initial chamber and the others to barrel locations which were swept by the projectile during the shot. Results are presented as time-resolved measurements of both the sensor temperature and the heat flux evaluated from equation 2 of the previous section.

In regions swept by the projectile the sensor will need to be inset to the wall to minimise possible mechanical damage due to the moving projectile. Tests were carried out to quantify the effect of radial positioning of the sensor on the wall and Figure 2 shows the result for three radial positions of the sensor at x = 2.88d. As can be seen, the differences between the temperatures of a flush mounted sensor and that inset by 0.2 mm to the wall are, on average, less than 5% which are within the temperature uncertainty of the system as discussed in Section 2. The differences at 0.6 mm inset, however, are appreciably larger, particularly at later times in the cycle with differences up to 25%. For subsequent measurements at locations swept by the projectile the sensor was inset to the wall by about 0.1 mm and, according to the conclusion of Figure 2, is expected to measure temperatures close to those of the wall surface.

Figure 3 shows the variation of the sensor temperature at x = 2.88d for five shots and indicates the expected uncertainty of the measurement system ($\pm$ 0.3^{o}C) and relatively good repeatability of the experiment from one shot to another.

The variations of the sensor temperature for the five axial locations considered are shown relative to the isentropic free-stream temperature in Figure 4 and in greater

detail in Figure 5. The temperature change of the sensor at all locations is less than $7^{o}C$, compared to that of the free-stream which reaches a temperature difference from the ambient of about $-140^{o}C$ at the end of the shot. At $x = 2.88d$, the temperature change shows a maximum of about $-5^{o}C$ at around 25 ms and thereafter recovers slightly to around $-4^{o}C$ towards the end of the cycle. At the other four locations, the temperature falls rapidly as the projectile passes over the sensor due to the expansion process in the gas behind the projectile and subsequently follows a moderate decrease during the rest of the shot, as shown in Figure 5. The sensor temperature is initially ambient at all locations and the deviations from zero in the first few ms of each trace, Figure 5, are within the experimental uncertainty of $\pm 0.3^{o}C$. The temperature change reached at the end of the shot reduces at locations further away from the breech to around $-6^{o}C$ at $x = 7.27d$ compared to $-5^{o}C$ at $x = 16.09d$. The scatter in each trace is within the uncertainty of the measurement system.

Heat transfer information can be obtained from the measured temperature record but the scatter in the temperature data results in a larger scatter in the heat flux as a consequence of the integration procedure performed according to equation 2. Polynomial curve-fit approximations at all five locations were made to remove the scatter and three of these are shown in Figure 6, and the resulting variations of heat flux and of heat transfer coefficient for the five locations in Figure 7.

The heat transfer coefficient is defined as

$$h = \frac{\dot{q}}{\Delta T} \qquad (3)$$

where ΔT is the temperature difference between the free-

stream and the wall-surface temperature which was assumed to be that of the sensor. In Figure 7a and at x = 2.88d, heat transfer from the wall to the fluid gradually increases from zero to around 1.8 10^4 W/m^2 at 17 ms and then gradually reduces to a value of 0.5 10^4 W/m^2 before the gas pressure is released at around 33 ms. At locations swept by the projectile (i.e. x = 7.27d, 10.21d, 13.15d and 16.09d) the heat transfer rapidly increases from zero as the projectile passes over the sensor and decreases virtually as rapidly to a value of around 1.6 10^4 W/m^2 for x = 7.27d and 10.21d. At x = 13.15d and 16.09d, the heat flux is larger and increases after 33 ms when the gas pressure was released. The convection coefficients in Figure 7b are consistent with those of heat flux so that, after the rapid decline, particularly at x = 7.27d, 10.21d and 13.15d, the heat transfer coefficient attains values ranging from around 70 W/m^2 ^oK at x = 2.88d to 220 W/m^2 ^oK at 16.09d.

Comparison between the convection coefficients of Figure 7b with those obtained from a correlation for a turbulent boundary layer over a flat plate with zero pressure gradient starting at the breech is helpful in determining the nature of the transient heat transfer process and of the corresponding thermal boundary layers. Figure 8 shows the convection coefficients for the five axial locations obtained from a correlation of reference 5, given by:

$$Nu = 0.0308\ Re^{4/5}\ Pr^{1/3} \qquad (4)$$

In applying the correlation above to the transient gun flow, quasi-steady flow assumption was made and Reynolds number and fluid properties were evaluated at each time step in the cycle using the corresponding velocity and pressure data of reference 1 and the isentropic free-stream and measured sensor temperature data of Figures 4 and 5.

The differences between the measured and correlation results at x = 7.27d, 10.21d, 13.15d and 16.09d are, as expected, large particularly in the early stages of the heat transfer process due mainly to the quasi-steady flow assumption. At x = 2.88d, the measured values in the first 2 ms of the shot are close to zero and rapidly increase over the next 3 ms as the flow goes through transition and becomes turbulent. The values attained are, however, higher by around 50% than the correlation results due mainly to the fact that the correlation takes no account of the favourable pressure gradient experienced by the flow, particularly in the early stages of the shot. As the flow develops and pressure gradients reduce later in the cycle, the measured values at x = 2.88d of Figure 7b approach the corresponding correlation results of Figure 8 and achieve values within 10%. At locations swept by the projectile, however, measured coefficients attain higher values throughout the cycle, for example up to 50% at x = 16.09d. These differences are thought to stem from the interaction of the projectile wake with the velocity boundary layer, in addition to the neglect of the pressure gradient in the correlation. There is, in fact, another boundary layer which develops at the base of the projectile and interacts with that growing from the breech, as reported in reference 1. The present results are consistent with the velocity results of reference 1 which showed that the measured boundary layers were generally thinner than those calculated for turbulent boundary layers with zero pressure gradient.

4. CONCLUSIONS

The main conclusions extracted from the preceding text can be summarised as follows:

1. A thin-film sensor with its surface 0.2 mm below that of the wall of the initial chamber indicated temperatures close to those of the sensor mounted flush on the wall and confirmed that measurements of heat flux at locations swept by the projectile were possible.

2. Heat transfer information was obtained by curve-fit approximations to the temperature records to remove scatter in the data and showed that the heat flux at various locations swept by the projectile decreased in time and increased with distance from the breech.

3. Comparison of the measured heat transfer coefficients with those obtained from a correlation for turbulent boundary layer with zero pressure gradient starting at the breech showed that the differences between the two cases were large at locations swept by the projectile due mainly to the neglect of the pressure gradient as well as to the effect of projectile wake on the boundary layer development. In the initial chamber, however, the wake effect is weak and the differences, although initially large, became progressively smaller as the pressure gradient reduced later in the shot.

ACKNOWLEDGEMENTS

Financial support provided by the US Army European Research Office is gratefully acknowledged. The technical assistance of Messrs J Laker, O Vis and P Trowell is also appreciated.

REFERENCES

1. A F Bicen, L Khezzar and J H Whitelaw
"Subsonic Single-Phase Flow in a Gun Simulator", to appear in AIAA Journal, 1987. Also a Mechanical Engineering Department Report, FS/86/03, Imperial College, 1986

2. A F Bicen, L Khezzar and J H Whitelaw
"Subsonic Single- and Two-Phase Flow Characteristics of a Gun Simulator", Mechanical Engineering Department Report, FS/86/43, Imperial College, 1986

3. M Schmidt
"Flow Characteristics of a Particle Loaded Gun Simulator", Mechanical Engineering Department Report, FS/87/29, Imperial College, 1987

4. D L Schultz and T V Jones
"Heat Transfer Measurements in Short-Duration Hypersonic Facilities", AGARD-AG-165, 1973

5. F P Incropera and D P DeWitt
"Fundamentals of Heat and Mass Transfer", John Wiley & Sons, Second Edition, 1985

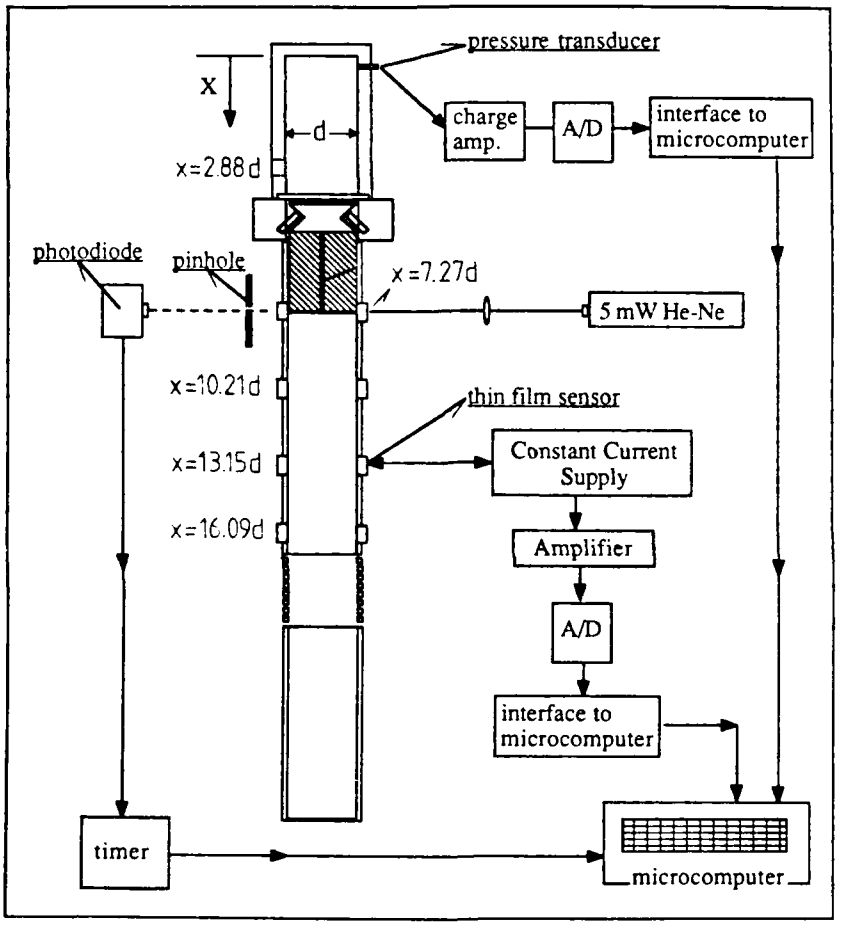

Figure 1 Experimental system

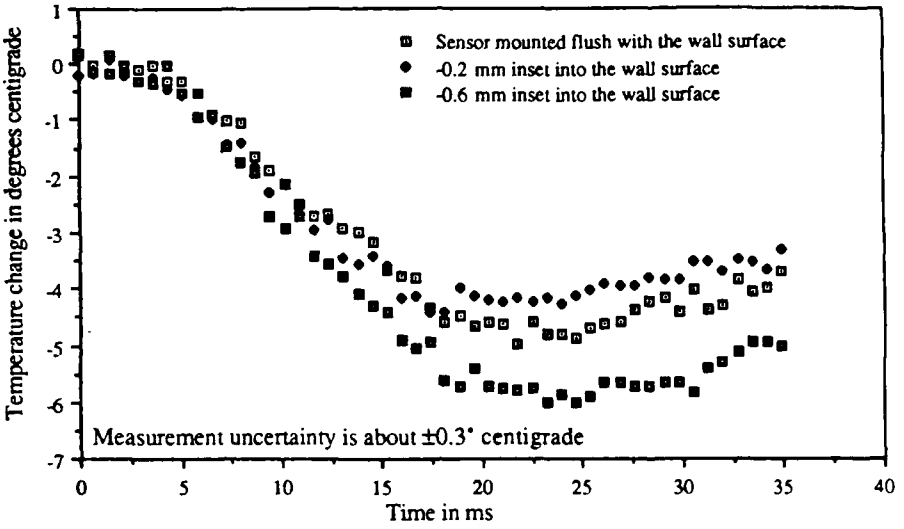

Figure 2 Effect of radial positioning of sensor on sensor temperature at x = 2.88d

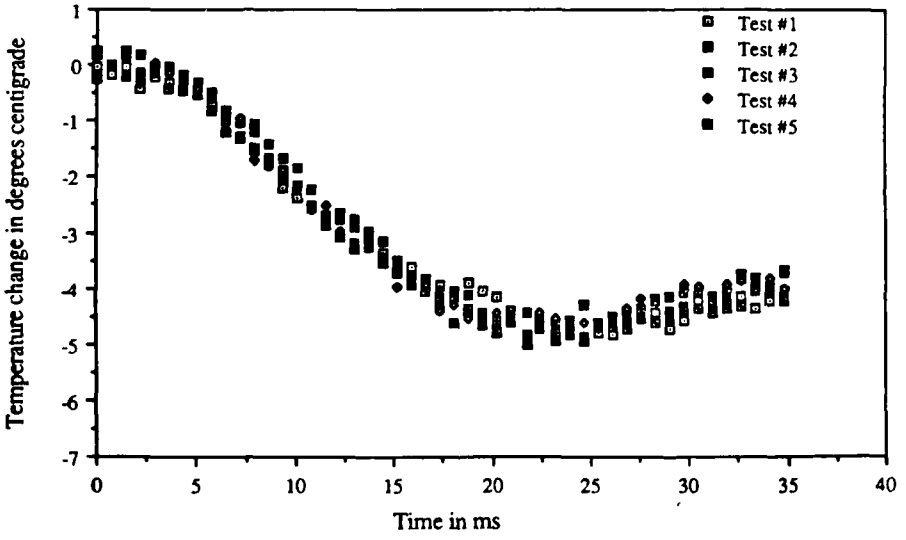

Figure 3 Sensor temperature variation at x = 2.88d over five shots

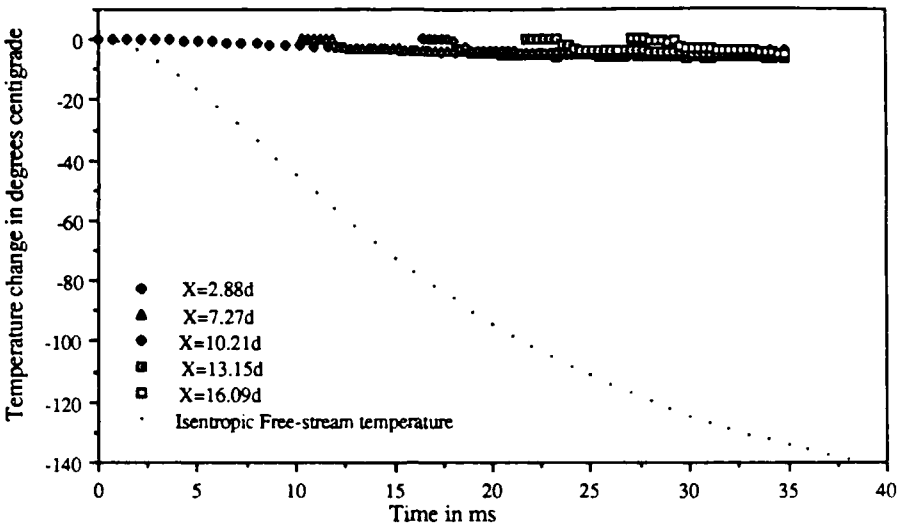

Figure 4 Sensor temperature at various axial locations relative to free-stream temperature

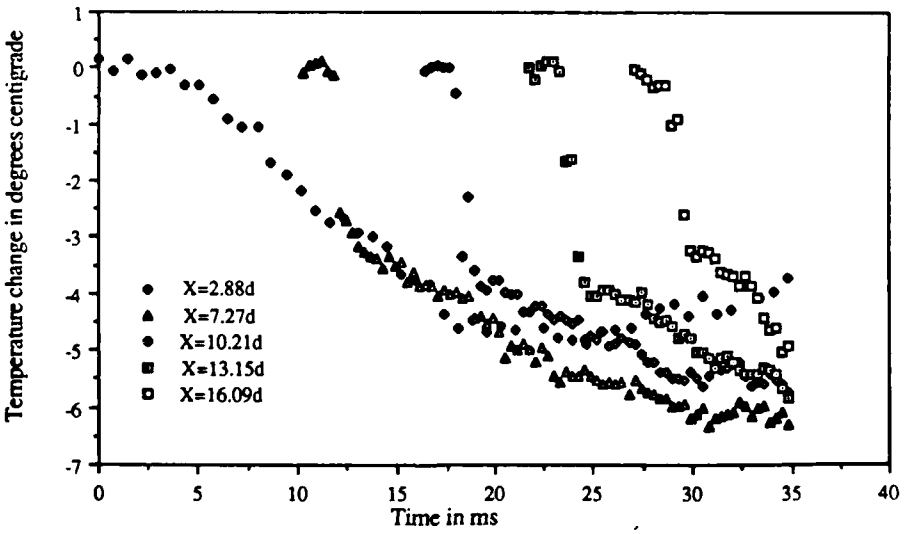

Figure 5 Sensor temperature at various axial locations

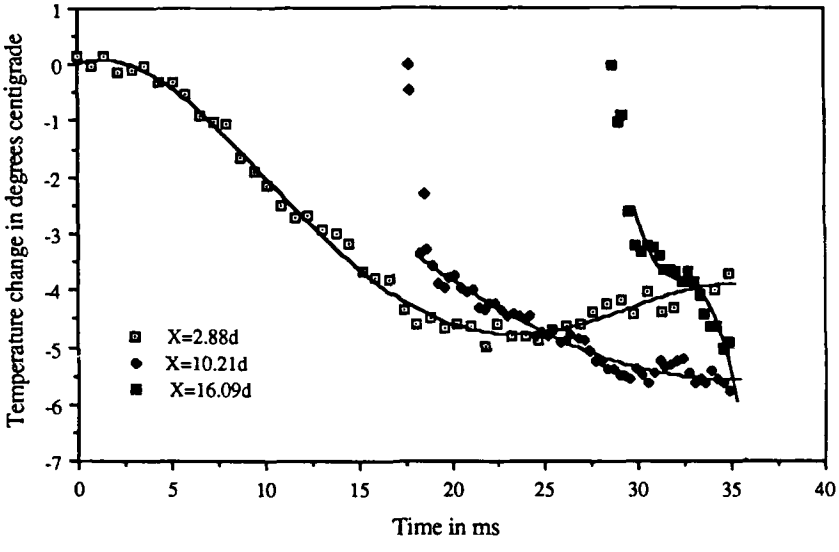

Figure 6 Curve-fit approximations to sensor temperature data

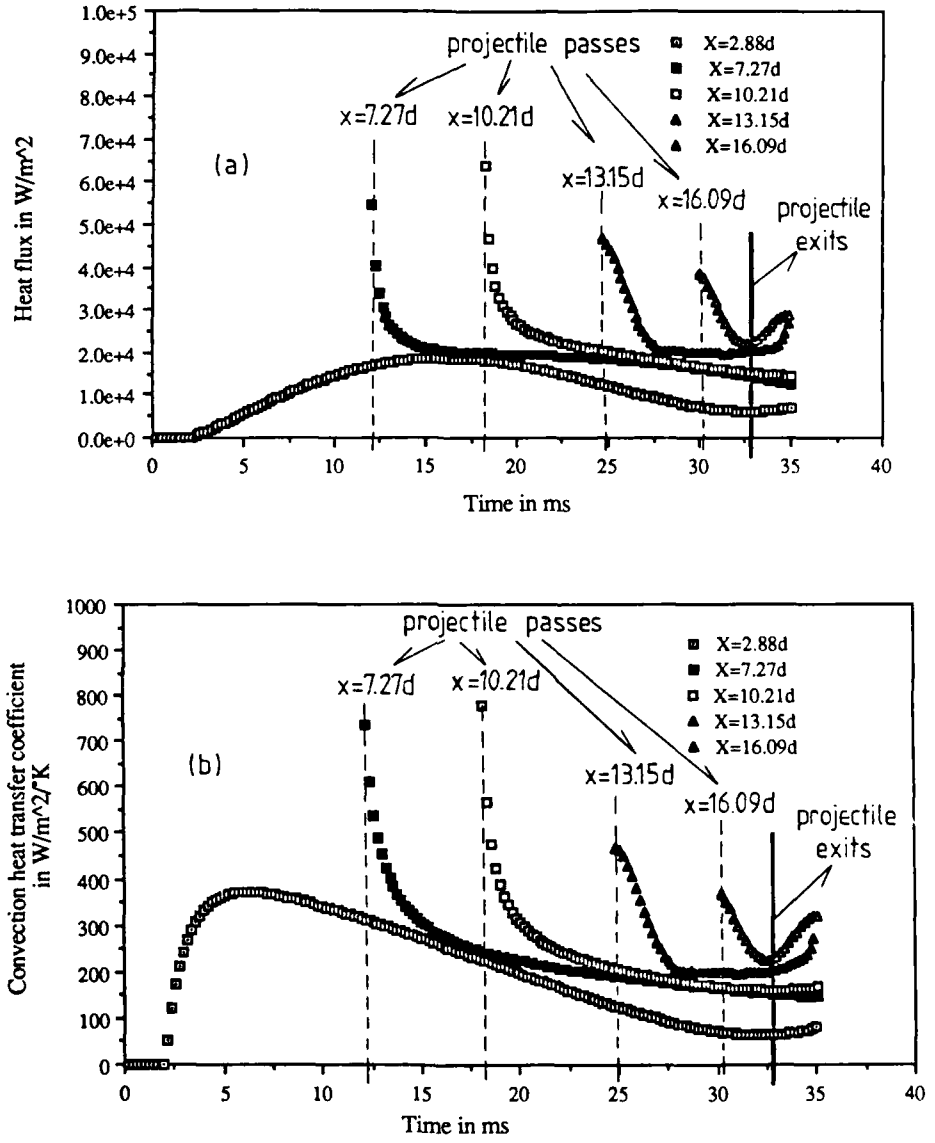

Figure 7 Heat flux and convection coefficient at various axial locations

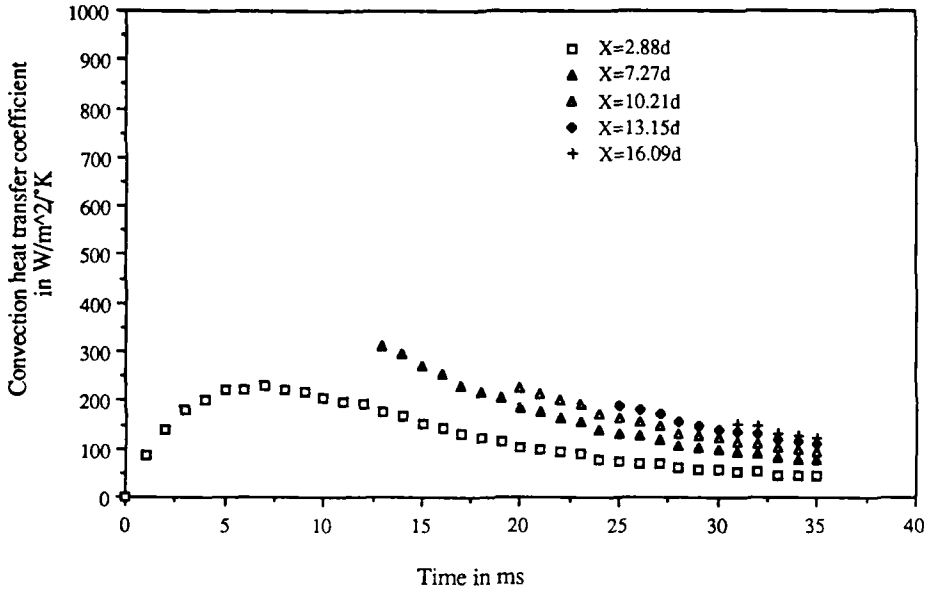

Figure 8 Convection coefficient at various axial locations evaluated from equation 4

END

DATE
FILMED

588